

Published in final edited form as:

*Acc Chem Res.* 2011 October 18; 44(10): 947–956. doi:10.1021/ar200022e.

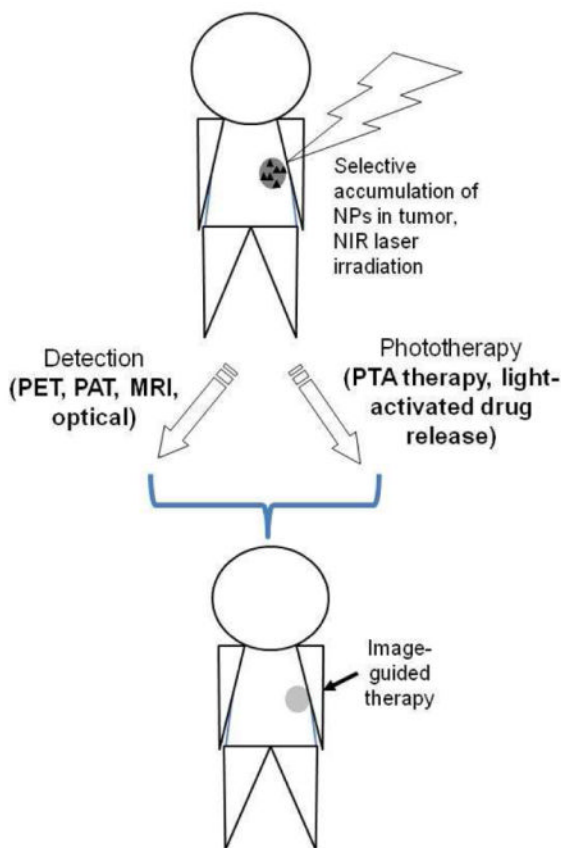
## Cancer Theranostics with Near-Infrared Light-Activatable Multimodal Nanoparticles

Marites P. Melancon, Min Zhou, and Chun Li\*

Departments of Experimental Diagnostic Imaging and Imaging Physics, The University of Texas MD Anderson Cancer Center, 1515 Holcombe Blvd., Houston, TX 77054

Marites P. Melancon: mmelancon@mdanderson.org; Min Zhou: mzhou1@mdanderson.org; Chun Li: cli@mdanderson.org

### CONSPECTUS



Nanomaterials that interact with light provide a unique opportunity for biophotonic nanomedicine. Multifunctional nanoparticles (NPs) that have strong and tunable surface plasmon resonance absorption in the near-infrared region combined with visibility with multiple imaging modalities (magnetic resonance imaging, nuclear imaging, and photoacoustic imaging) have great potential in image-guided therapies. These novel nanostructures, once introduced, are expected to home to solid tumors via the enhanced permeability and retention effect (a passive targeting mechanism) or

\*CORRESPONDING AUTHOR: Department of Experimental Diagnostic Imaging, Unit 59, The University of Texas MD Anderson Cancer Center, 1515 Holcombe Boulevard, Houston, Texas 77030. Phone: (713) 792-5182. Fax: (713) 794-5456.

via targeting ligands bound to their surfaces (an active targeting mechanism). The primary mode of action for photothermal conducting NPs is to convert photoenergy into heat, causing temperature in the treatment volume to be elevated above the thermal damage threshold, which results in irreversible cell killing. It is now recognized that this process, termed photothermal ablation therapy or PTA, although very effective, is unlikely to kill all tumor cells when used alone. In addition to PTA, photothermal conducting NPs can also efficiently trigger drug release and activate RNA interference. Such a multimodal approach, which permits simultaneous PTA therapy, chemotherapy, and therapeutic RNA interference, should provide an opportunity for complete eradication of residual disease.

In this Account, we provide an up-to-date review of the synthesis and characterization, functionalization, and in vitro and in vivo evaluation of NIR light-activatable multifunctional nanostructures used for imaging and therapy, with an emphasis on hollow gold nanospheres, magnetic core-shell gold nanoshells, and semiconductor copper monosulfide NPs. We discuss three types novel drug delivery systems in which hollow gold nanospheres are used to mediate controlled drug release.

## Keywords

Theranostics; hollow gold nanospheres; copper sulfide nanoparticles; near-infrared; drug delivery

## 1. Introduction

Two unique features distinguish nanoparticles (NPs) from small-molecular-weight compounds used in cancer theranostics. First, certain NPs possess unique physicochemical properties that can be harnessed for both diagnostic and therapeutic applications. Second, multiple functions can be readily integrated into a single nanostructure, enabling the design of NPs for multimodal image-guided therapy. An example of NPs with unique physicochemical properties is photothermal conducting agents used in photothermal ablation (PTA) therapy.

PTA has gained popularity recently because a specific amount of photoenergy is delivered directly into the tumor mass without causing systemic effects, thus promising minimally invasive intervention as an alternative to surgery.<sup>1</sup> Depending on the temperature achieved, photothermal therapy produces either hyperthermia or PTA. Hyperthermia is the heating of tissues to 42–46°C;<sup>2</sup> irreversible PTA-induced necrosis occurs when tissues are heated to 43°C for 240 min, which is equivalent to 54°C for 1 s.<sup>3</sup> PTA has been used successfully to ablate tumors throughout the body.<sup>1,4,5</sup>

Because the heating achieved by converting laser energy into thermal energy is nonspecific, treatment volume and exposure time are limited by potential damage to the surrounding normal tissues. To improve the efficacy and tumor selectivity of laser-induced PTA, light-absorbing photothermal conducting NPs are introduced into tumors. Ideal NPs for PTA should have strong and tunable absorption in the near-infrared (NIR) region, have low toxicity, and be amenable to surface conjugation to actively target cancer cells. Absorption of NIR light (650–1064 nm) is desirable for optimal tissue penetration.<sup>6</sup> To date, most photothermal conducting agents have been based on various gold (Au) nanostructures, including nanoshells, nanorods, and nanocages.<sup>7–9</sup> Silica-cored Au nanoshells have advanced into clinical trials under the brand name AuroLase.

Successful PTA therapy requires (i) selective delivery of enough photothermal conducting NPs to tumor tissue to mediate effective PTA of tumor cells without damaging the surrounding normal tissues, (ii) accurate pretreatment thermal dose calculation, and (iii)

noninvasive real-time monitoring of the spatiotemporal heat profile and response to therapy in a given target volume. Particle size is the most important physicochemical factor influencing the tumor targeting efficiency of NPs.<sup>10</sup> Smaller NPs have a better chance of achieving both passive and active targeting because of increased extravasation and enhanced interstitial transport. Recently, significant progress has been made in designing photothermal conducting NPs with an average diameter  $d < 100$  nm. These include hollow Au nanospheres (HAuNSs), with  $d = 30\text{--}50$  nm,<sup>11,12</sup> and copper monosulfide (CuS) NPs, with  $d = \sim 2\text{--}15$  nm.<sup>13,14</sup>

Another consideration in designing photothermal conducting NPs with improved performance is the integration of imaging capability. This approach is exemplified by Au nanoshells containing superparamagnetic iron oxide (SPIO) NPs; these nanostructures have both optical and magnetic properties.<sup>15</sup> Because PTA-induced tissue necrosis can be estimated using thermal damage models such as that of Sapareto and Dewey,<sup>3</sup> it is envisioned that if the intratumoral distribution of magnetic photothermal conducting NPs can be quantified using magnetic resonance imaging (MRI) by measuring changes in  $T_2^*$  relaxivity, it will be possible to simulate the heat profile and thus predict the effect of PTA therapy.<sup>16</sup> During PTA therapy, magnetic resonance temperature imaging (MRTI) can be used to map the spatiotemporal temperature profile.<sup>17</sup> This and other noninvasive imaging techniques can be used in treatment planning before PTA therapy to ensure accurate delivery of heat to the treatment volume while avoiding the surrounding critical structures. Imaging techniques can also be used to assess the extent of PTA therapy to provide crucial feedback about safety and efficacy.

NIR laser-modulated photothermal effects have enabled novel drug delivery systems to be designed not only mediate PTA of tumor cells but also activate the release of anticancer agents. PTA therapy alone is unlikely to kill all tumor cells because the heat distribution is nonuniform, especially in areas peripheral to large blood vessels where heat can be rapidly dissipated by circulating blood. Combining PTA therapy with simultaneous NIR laser-activated chemotherapy and/or RNA interference (RNAi) should provide an opportunity for complete eradication of residual disease.

In this Account, we provide an up-to-date review of NIR light-activatable multifunctional nanostructures used in cancer theranostics and drug delivery, focusing on the recent development of HAuNSs, magnetic core-shell Au nanostructures, and CuS NPs. We discuss three types of novel drug delivery systems integrating HAuNS as a photothermal conducting mediator. Figure 1 summarizes the structures and functions of these NPs. Excellent reviews about silica-cored Au nanoshells, nanorods, and nanocages can be found elsewhere.<sup>18–20</sup>

## 2. Hollow Gold Nanospheres

Nanostructures made of Au and silver (Ag) exhibit a tunable optical phenomenon termed surface plasmon resonance (SPR). When exposed to light, the conduction electrons in a metal nanostructure are driven by the electric field to collectively oscillate at a resonance frequency relative to the lattice of positive ions. At this resonance frequency, the incident light is absorbed by the nanostructure. For solid spherical NPs, the resonance is at  $\sim 520$  nm for Au and  $\sim 400$  nm for Ag; the peak wavelength varies slightly depending on the NP size and the embedding medium. The SPR peak can be tuned from visible to NIR by varying the size, shape, and structure of the NPs. HAuNSs, novel Au nanostructures consisting of only a thin Au wall with a hollow interior, have the unique combination of small size, spherical shape, hollow interior, and a strong and tunable absorption band in the NIR region as a result of their highly uniform structure.

## 2.1. Synthesis and Characterization

Liang et al. first reported the synthesis of HAuNSs with tunable interior-cavity sizes by using cobalt (Co) NPs as sacrificial templates.<sup>21</sup> As reduction potential of  $\text{AuCl}_4^-/\text{Au}$  redox couple (0.935 V vs the standard hydrogen electrode [SHE]) is much higher than that of  $\text{Co}^{2+}/\text{Co}$  redox couple (-0.377 V vs SHE),  $\text{AuCl}_4^-$  is readily reduced to Au atoms as soon as Co NPs are added into chloroauric acid solution:  $3\text{Co} + 2\text{AuCl}_4^- = 2\text{Au} + 3\text{Co}^{2+} + 8\text{Cl}^-$ . The reduced Au atoms nucleate, grow into very small particles, and eventually evolve into a thin shell around the Co NPs. The shells have an incomplete porous structure at an early stage when  $\text{Co}^{2+}$  and  $\text{AuCl}_4^-$  can continuously diffuse across the shell in opposite directions. When  $\text{AuCl}_4^-$  has been completely consumed, the remaining Co “core” is continually oxidized by  $\text{H}^+$  in aqueous solution (the reduction potential of the  $\text{H}^+/\text{H}_2$  redox couple is 0.0 V vs SHE). Shell formation is an inward growth process, in which the thickness of the Au shell increases inwards as the replacement between Co NPs and  $\text{HAuCl}_4$  continues. Therefore, the outer diameter is controlled by the diameter of the Co NPs, whereas the interior-cavity size is controlled by the stoichiometric ratio of  $\text{HAuCl}_4$  and the reducing agents. In addition to Co NPs, Ag NPs have also been used as sacrificial templates in the synthesis of HAuNSs.<sup>22</sup>

## 2.2. Functionalization

Homing ligands can be conveniently conjugated to the Au surface of HAuNSs through covalent bonds using SH-terminated compounds. Various homing ligands have been conjugated on the surface of HAuNSs, including peptides,<sup>11</sup> antibodies,<sup>12</sup> and low-molecular-weight organic compounds.<sup>23</sup> HAuNSs are usually stabilized with polyethylene glycol (PEG). Au NPs coated with higher molecular weight (5 kDa) PEG are more stable than those coated with lower molecular weight (2 kDa) PEG, and Au NPs coated with thioctic acid-anchored PEG that contains two thiol groups have higher colloidal stability in aqueous solution than Au NPs coated with monothiol-anchored PEG.<sup>10-12,23</sup>

## 2.3. Imaging

An emerging imaging modality that uses NIR light-absorbing NPs is photoacoustic tomography (PAT). PAT is a hybrid technology that images the internal distribution of optical energy deposition in biological tissues by detecting laser-induced ultrasonic waves (photoacoustic or optoacoustic waves).<sup>24</sup> PAT provides higher spatial resolution in deep tissues than traditional optical imaging because ultrasonic scattering is 2 orders of magnitude less than optical scattering in such tissues. PAT has been successfully applied to the visualization of different tissue structures and has been especially useful in imaging the cerebral cortex in small animals. As PAT is an absorption-based technique, the high absorption coefficient of HAuNSs makes them an excellent contrast agent. We have demonstrated excellent clarity and detail in PAT images of blood vessels in the brains of mice at 2 h after intravenous injection of long-circulating PEGylated HAuNSs.<sup>25</sup> Moreover, molecular PAT imaging with cyclic Arg-Gly-Asp (RGD) peptide-tagged HAuNSs targeted to integrin  $\alpha v \beta 3$  was successfully demonstrated in an orthotopic U87 glioma.<sup>26</sup> Targeted HAuNSs may be used as a single nanoplatform for PAT image-guided PTA.

The in vivo biodistribution and clearance of HAuNSs can also be noninvasively monitored by tagging the NPs with radioisotopes. For instance, positron emitters (e.g.,  $^{64}\text{Cu}$ ) have been conjugated to the surface of HAuNSs for positron emission tomography (PET) imaging.<sup>23</sup>

## 2.4. Therapy

HAuNSs are ideally suited as photothermal coupling agents for targeted delivery after systemic administration. Their smaller size ( $d \approx 40$  nm) compared with silica-cored Au

nanoshells ( $d > 120$  nm) permits greater extravasation from tumor blood vessels, whereas their strong light absorption and narrow SPR band are important for PTA as these properties directly affect heat-converting efficiency. To achieve targeted delivery, we conjugated C225, a monoclonal antibody directed at epidermal growth factor receptor (EGFR), to HAuNSs (C225-HAuNSs). In vitro, we observed EGFR-mediated selective uptake of the resulting conjugate C225-HAuNS, but not the IgG-HAuNSs control, in EGFR-positive A431 tumor cells. Irradiation of A431 cells treated with C225-HAuNSs plus NIR laser (40 W/cm<sup>2</sup> for 5 min) resulted in selective destruction of these cells. In contrast, treatment with C225-HAuNSs alone, laser alone, or IgG-HAuNSs plus NIR laser did not result in any observable effect on cell viability (Figure. 2).<sup>12</sup>

In addition to antibodies, HAuNSs have also been conjugated with a low-molecular-weight peptide, [Nle<sup>4</sup>, D-Phe<sup>7</sup>] $\alpha$ -MSH (NDP-MSH), as a targeting moiety through a PEG linker.<sup>11</sup> NDP-MSH is a potent agonist of melanocortin type-1 receptor, which is overexpressed in many melanoma cells, and binds to the receptor with high affinity (IC<sub>50</sub> = 0.21 nM).<sup>27</sup> The tumor uptake of NDP-MSH-conjugated HAuNSs was significantly higher than that of control PEGylated HAuNSs without peptide conjugation ( $12.6 \pm 3.1\%$  ID/g vs  $4.3 \pm 1.2\%$  ID/g) at 4 h after intravenous injection in B16/F10 melanoma-bearing nude mice (Figure 3A).<sup>11</sup> This suggests that the targeted HAuNSs had enhanced extravasation from tumor blood vessels and increased dispersion into the tumor matrix (Figure 3B). Furthermore, the PTA effect of NPs was confirmed both histologically, and functionally, by [<sup>18</sup>F]fluorodeoxyglucose PET.<sup>11</sup> The successful active targeting of NDP-MSH-conjugated HAuNSs to melanoma suggests their potential application in targeted PTA for melanoma.

### 3. Magnetic Core–Shell Au Nanostructures

MRI is a widely used modality in cancer theranostics because of its high spatial and temporal resolution, lack of ionizing radiation, and relatively high detection sensitivity compared with computed tomography. Several SPIO-based MRI contrast agents have been approved for human use or are in clinical trials.<sup>28</sup> Therefore, nanostructures combining the magnetic properties of SPIO and the optical properties of Au nanoshells are expected to provide a novel approach for simultaneous diagnostic imaging and PTA of cancer.

#### 3.1. Synthesis and Characterization

Multifunctionality is achieved by synthesizing Au nanostructures of different core structures and shapes.<sup>29</sup> For example, Kim et al. synthesized a nanostructure with a silica core, an Au shell, and a layer of SPIO sandwiched between silica and Au.<sup>30</sup> The synthesis involves three stages: formation of SPIO-coated silica, nucleation (i.e., small Au nanocrystal formation), and growth. In addition to silica, other materials, such as organic polymers, have also been used as dielectric interface between magnetic iron oxide core and Au shell.<sup>31</sup> Wang et al. reported a novel Au-coated magnetic NP, shaped like a grain of rice, that displays two distinct absorptions, from transverse and longitudinal plasmons.<sup>32</sup> These Au-shelled magnetic NPs all have  $d \geq 200$  nm.

To synthesize magnetic Au nanostructures with  $d < 100$  nm, Ji et al. used silica as dielectric interface, with SPIO NPs embedded inside a silica core (SPIO@silica-Au NP).<sup>15</sup> In a typical reaction scheme, SPIO NPs are coated with silica via the classic Stober sol-gel process.<sup>33</sup> The silica-coated SPIO NPs are then functionalized with amino groups. Next, Au nanocrystal seeds ( $d = 2-3$  nm) are attached to the amino groups on the silica sphere. Finally, the attached Au nanoseeds are used to nucleate the growth of an Au layer on the silica surface to form an Au nanoshell. Extensive structural and magnetic characterization have confirmed the presence of  $\gamma$ -Fe<sub>2</sub>O<sub>3</sub> cores in SPIO@silica-Au NPs.<sup>34</sup> SPIO@silica-Au

NPs exhibited high transverse relaxivity  $r_2$  and a large  $r_2/r_1$  ratio and therefore could be imaged by MRI to obtain  $T_2^-$  weighted images.<sup>15</sup>

### 3.2. Functionalization

Tumor-cell-specific ligands have been successfully conjugated onto the surface of SPIO-embedded Au nanoshells using essentially the same chemistry as used to modify the surface of other Au nanostructures. For example, anti-HER2 antibody was conjugated onto the surface of SPIO-embedded Au nanoshells and was shown to target and mediate selective killing of tumor cells through PTA in vitro.<sup>30</sup> We showed selective cell killing in vitro and significantly increased tumor uptake in vivo after systemic injection with SPIO@silica-Au NPs coated with an anti-EGFR monoclonal antibody.<sup>35</sup>

### 3.3. Imaging and Therapy

The promise of Au-shelled magnetic nanostructures is their multifunctionality for targeted delivery, diagnosis, and imaging guidance. So far, in vivo studies using these NPs have been very limited. Our preliminary in vivo data show that SPIO@silica-Au NPs mediated an efficient photothermal effect in nude mice implanted with tumor, because of their strong absorption in the NIR region, whereas the presence of SPIO provided contrast in  $T_2^*$  MRI of the tumor (Figure 4A).<sup>36</sup> Our data indicate that upon intratumoral injection of SPIO@silica-Au NPs in mice bearing A431 tumors and subsequent treatment with 808-nm laser, the tumor temperature increased to 65°C, significantly higher than 44°C obtained when the tumors were injected with saline (Figure 4B,C).<sup>36</sup> These data suggest that MRI should be useful for assessing SPIO@silica-Au NP intratumoral distribution, which in turn may be used to plan PTA therapy and predict treatment outcome. In addition to MRI, magnetic SPIO NPs can also mediate increased tumor accumulation of NPs in the presence of an external magnetic field at the target site.<sup>36</sup>

## 4. Copper Sulfide Nanoparticles

CuS NPs are a new class of promising photothermal coupling agents that have SPR peaks in the NIR region (~900–1100 nm).<sup>14,37</sup> These NPs are much smaller ( $d < 15$  nm) than plasmonic Au nanostructures with SPR peaks in the NIR region and therefore have a better chance of reaching their targets and being cleared from the body through the renal system.<sup>38</sup> An interesting approach was devised to incorporate  $^{64}\text{Cu}$  into the matrix of CuS NPs. These  $^{64}\text{Cu}$ -labeled multifunctional NPs have been shown to mediate PTA therapy and also permit PET imaging and radiotherapy.<sup>14</sup>

### 4.1. Synthesis

CuS NPs are readily synthesized in aqueous solution by reacting  $\text{CuCl}_2$  and  $\text{Na}_2\text{S}$  in the presence of various stabilizers.  $^{64}\text{CuCl}_2$  may be added into the reaction solution to obtain chelator-free [ $^{64}\text{Cu}$ ]CuS NPs with extremely high specific activity. PEG is coated onto the surface of CuS NPs by incubating CuS NPs with SH-PEG at room temperature.<sup>14</sup>

### 4.2. Imaging

Because of their strong absorption in the NIR region, CuS NPs are well suited for PAT imaging. Preliminary PAT studies were conducted with CuS NPs dispersed in 10% polyacrylamide gel embedded in fresh chicken breast tissues. The gel phantom could be clearly visualized at ~5 cm depth from the laser illuminating surface.<sup>39</sup>

[ $^{64}\text{Cu}$ ]CuS NPs were also used as radiotracers for biodistribution and microPET imaging studies.  $^{64}\text{Cu}$  ( $t_{1/2}$ , 12.7 h;  $\beta^+$ , 0.653 MeV [17.8%];  $\beta^-$ , 0.579 MeV [38.4%]) has decay characteristics that allow for both PET imaging and targeted radiotherapy for cancer.<sup>40</sup>

Tumor uptake was almost 3 times as high with PEGylated [<sup>64</sup>Cu]CuS NPs as with citrate-coated [<sup>64</sup>Cu]CuS NPs at 24 h after intravenous injection (7.6 vs 2.6% ID/g,  $P = 0.011$ ) in human U87 glioma xenografts.<sup>14</sup> This can be attributed to enhanced permeability and retention effect of the NPs and greater systemic exposure of long-circulating PEG-[<sup>64</sup>Cu]CuS NPs. Figure 5A shows representative whole-body microPET/CT images of a mouse acquired at 24 h after intravenous injection of PEG-[<sup>64</sup>Cu]CuS NPs. As expected, these NPs accumulated in the tumor, permitting remarkably clear visualization of the tumor.<sup>14</sup>

### 4.3. Therapy

PTA of tumor cells incubated with CuS NPs has been demonstrated *in vitro* and *in vivo*.<sup>14,37</sup> Histologic examination confirmed that the combination of PEG-CuS NPs administered by either intratumoral or intravenous injection followed by laser treatment caused a significantly greater necrotic response than did PEG-CuS NPs without laser, saline plus laser, or saline only (Figure 5B). In mice treated with PEG-CuS NPs plus laser, common features of thermonecrosis, such as loss of nucleus, cell shrinkage, and coagulation, were found in the tumor tissues. These studies confirmed selective *in vivo* PTA destruction of the tumor cells mediated by PEG-CuS NPs.

## 5. NIR Light-Activatable Drug Release from Hollow Gold Nanospheres

HAuNSs can be classified into three categories according to how drugs are loaded: drugs may be (i) loaded inside the hollow interior of HAuNSs;<sup>41</sup> (ii) conjugated to the surface of HAuNSs;<sup>23</sup> or (iii) co-loaded to soft matrix, such as polymeric microspheres or liposomes (Figure 6).<sup>42,43</sup> This approach is a promising anticancer strategy because it permits simultaneous PTA therapy, chemotherapy, and therapeutic RNAi; is expected to significantly increase the likelihood of cell killing; and may overcome resistance to chemotherapeutic agents. Depending on the laser source, NIR-light-activated drug release systems can be further divided into two modes: those using continuous-wave laser and those using high-energy pulsed laser to activate drug release.

### 5.1. Trapping DOX Inside HAuNSs

To demonstrate the feasibility of laser-modulated drug release, we loaded doxorubicin (DOX) inside HAuNSs.<sup>41</sup> Up to 63% DOX by weight (~1.7 μg DOX/μg Au) could be loaded into PEG-coated HAuNSs. Irradiation with continuous NIR laser triggered rapid DOX release from DOX-loaded HAuNSs. When MDA-MB-231 cells incubated with DOX-loaded HAuNSs (DOX@PEG-HAuNSs) were irradiated with NIR light, significantly greater cell killing than with free DOX alone was observed; this is attributable to both HAuNS-mediated hyperthermia and thermal sensitization of cells to DOX. *In vivo*, systemic administration of DOX@PEG-HAuNSs followed by NIR laser had greater antitumor activity in a xenograft model of breast cancer than free DOX alone, DOX@PEG-HAuNSs alone, liposomal DOX, or NIR irradiation alone (unpublished data). Three of six tumors treated with DOX@PEG-HAuNSs plus NIR laser disappeared completely. Moreover, DOX@PEG-HAuNSs showed lower systemic toxicity than free DOX or liposomal DOX. The estimated maximum tolerated doses for free DOX, liposomal DOX, and DOX@PEG-HAuNSs were ~15, ~30, and >60 mg equivalent DOX/kg, respectively. These results suggest that multimodal treatment approach mediated by an activatable drug delivery system can significantly increase the likelihood of cell killing with less systemic toxicity.

### 5.2. siRNA Delivery

Small interfering RNA (siRNA) molecules are short, double-stranded RNA molecules that target specific complementary mRNAs for degradation via RNAi, which can induce

posttranscriptional gene silencing.<sup>44</sup> The emphasis on RNAi approaches is justified because many important cancer therapy targets are difficult to inhibit with small molecules, which also require a lengthy development phase and often fail. We have developed an innovative technology that permits NIR laser-induced RNAi using HAuNSs.<sup>23</sup> Successful implementation of this new technique would have the enormous advantage of confining RNAi to the illuminated area, reducing nonspecific and off-target effects. We conjugated siRNA directed at NF- $\kappa$ B p65 subunit to HAuNSs. MicroPET/CT images of mice bearing HeLa tumors showed significantly higher tumor uptake of folic acid (FA)-conjugated nanoparticles <sup>64</sup>Cu-labeled FA-HAuNS-siRNA<sub>NF- $\kappa$ B</sub> (targeting to folate receptors) than of nontargeted HAuNS-siRNA<sub>NF- $\kappa$ B</sub> control (Figure 7A). Effective silencing of NF- $\kappa$ B p65 in vivo was observed only in the tumors irradiated with nanosecond pulsed NIR laser, demonstrating that HAuNSs can mediate efficient RNAi (Figure 7B,C).

### 5.3. Microspheres Loaded with Paclitaxel and HAuNSs

To evaluate the feasibility of NIR-light-modulated drug release from microspheres, we prepared microspheres containing paclitaxel (PTX) and HAuNS (PTX/HAuNS-MS) from biocompatible, biodegradable poly(lactic acid-co-glycolic acid) (PLGA) using a modified water-in-oil-in-water (W1/O/W2) double-emulsion solvent evaporation method.<sup>42</sup> These PLGA microspheres elevated the temperature of water to the same extent as did HAuNSs in water having the same concentration of nanoparticles, indicating that PLGA polymer matrix did not prevent NIR light from reaching HAuNS embedded in the microspheres. We further demonstrated that the amount of PTX released from these microspheres could be modulated by controlling the laser output power and HAuNSs concentration. Significant differences were found in the cell-killing effect of PTX/HAuNS-MS with and without NIR irradiation. When cells were incubated with PTX/HAuNS-MS at microsphere concentrations of 1 mg/ml and 10 mg/ml but were not exposed to NIR irradiation, 86.5% and 67.4% of the cells, respectively, were viable after 72 h of incubation. However, when cells were incubated with PTX/HAuNS-MS at the same microsphere concentrations and exposed to NIR irradiation, only 38.8% and 3.9% of the cells, respectively, were viable after 72 h.<sup>42</sup> Our data support the idea that the combination of photothermal effect from HAuNSs and chemotherapy is more efficient than photothermal effect alone in killing tumor cells.

The 3 drug delivery systems are suitable for different applications. Microspheres loaded with HAuNS and anticancer agents can be used for chemoembolization in the treatment of liver cancer or for intratumoral injection. This delivery system is applicable to a wide range of drugs. On the other hand, physical entrapment of drugs in HAuNSs is simple and straightforward, but is limited to charged, low-molecular-weight drugs amendable to drug loading. The siRNA delivery system permits controlled gene silencing and promises reduced systemic toxicity. Physical entrapment and siRNA delivery systems can both be administered systemically, making it possible for targeting metastatic disease.

In principle, the NIR light-activatable drug release systems used with HAuNSs may be adapted with other photothermal conducting agents, such as CuS NPs and magnetic core-shell Au nanostructures.

## 6. Conclusions and Perspectives

Multifunctional photothermal conducting NPs permit simultaneous cancer diagnosis and therapy. Depending on the particular application, multiple treatment modalities can be integrated into a single nanostructure design, enabling the possibility of completely eradicating cancer cells using a combination of PTA therapy, chemotherapy, radiotherapy, and therapeutic RNAi. As these NPs are readily visualized with MRI, PET, and PAT, they

are particularly suited for image-guided therapies. One can envision a myriad of potential applications in cancer theranostics using these “see-and-treat” strategies.

Before these new nanomaterials are tested in cancer patients, detailed preclinical studies should be conducted, especially to investigate the pharmacokinetics, in vivo tumor targeting, and therapeutic effects of these NPs. Furthermore, the clearance of the Au NPs and their acute and long-term toxicity need to be examined thoroughly. These NPs should meet the safety, effectiveness, and quality control standards of new drug development.

## Acknowledgments

We thank Karen Muller for editing the manuscript. This work was supported in part by grants from the National Institutes of Health (grants R01 CA119387, CA119387-05S1, and U54CA151668, and MD Anderson’s Cancer Center Support Grant CA016672), the John S. Dunn Foundation, SPOR Head and Neck Career Development Award P50CA097007 (to M.P.M.), and an Odyssey Fellowship (to M.P.M.). The small-animal imaging studies were partially funded by the Experimental Cancer Imaging Research Program, funded by NCI (U24 CA126577).

## References

1. Fiedler VU, Schwarzmaier HJ, Eickmeyer F, Muller FP, Schoepp C, Verreet PR. Laser-induced interstitial thermotherapy of liver metastases in an interventional 0.5 Tesla MRI system: technique and first clinical experiences. *J Magn Reson Imaging*. 2001; 13:729–737. [PubMed: 11329194]
2. Overgaard J, Gonzalez Gonzalez D, Hulshof MC, Arcangeli G, Dahl O, Mella O, Bentzen SM. Randomised trial of hyperthermia as adjuvant to radiotherapy for recurrent or metastatic malignant melanoma. *European Society for Hyperthermic Oncology. Lancet*. 1995; 345:540–543. [PubMed: 7776772]
3. Sapareto SA, Dewey WC. Thermal dose determination in cancer therapy. *Int J Radiat Oncol Biol Phys*. 1984; 10:787–800. [PubMed: 6547421]
4. Rosenberg C, Puls R, Hegenscheid K, Kuehn J, Bollman T, Westerholt A, Weigel C, Hosten N. Laser ablation of metastatic lesions of the lung: long-term outcome. *Am J Roentgenol*. 2009; 192:785–792. [PubMed: 19234278]
5. Lindner U, Weersink RA, Haider MA, Gertner MR, Davidson SR, Atri M, Wilson BC, Fenster A, Trachtenberg J. Image guided photothermal focal therapy for localized prostate cancer: phase I trial. *J Urol*. 2009; 182:1371–1377. [PubMed: 19683262]
6. Weissleder R. A clearer vision for in vivo imaging. *Nat Biotechnol*. 2001; 19:316–7. [PubMed: 11283581]
7. Hirsch LR, Stafford RJ, Bankson JA, Sershen SR, Rivera B, Price RE, Hazle JD, Halas NJ, West JL. Nanoshell-mediated near-infrared thermal therapy of tumors under magnetic resonance guidance. *Proc Natl Acad Sci USA*. 2003; 100:13549–13554. [PubMed: 14597719]
8. Skrabalak SE, Au L, Lu X, Li X, Xia Y. Gold nanocages for cancer detection and treatment. *Nanomed*. 2007; 2:657–668.
9. Huang X, El-Sayed IH, Qian W, El-Sayed MA. Cancer cell imaging and photothermal therapy in the near-infrared region by using gold nanorods. *J Am Chem Soc*. 2006; 128:2115–2120. [PubMed: 16464114]
10. Zhang G, Yang Z, Lu W, Zhang R, Huang Q, Tian M, Li L, Liang D, Li C. Influence of anchoring ligands and particle size on the colloidal stability and in vivo biodistribution of polyethylene glycol-coated gold nanoparticles in tumor-xenografted mice. *Biomaterials*. 2009; 30:1928–1936. [PubMed: 19131103]
11. Lu W, Xiong C, Zhang G, Huang Q, Zhang R, Zhang JZ, Li C. Targeted photothermal ablation of murine melanomas with melanocyte-stimulating hormone analog-conjugated hollow gold nanospheres. *Clin Cancer Res*. 2009; 15:876–886. [PubMed: 19188158]
12. Melancon MP, Lu W, Yang Z, Zhang R, Cheng Z, Elliot AM, Stafford J, Olson T, Zhang JZ, Li C. In vitro and in vivo targeting of hollow gold nanoshells directed at epidermal growth factor receptor for photothermal ablation therapy. *Mol Cancer Ther*. 2008; 7:1730–1739. [PubMed: 18566244]

13. Li YB, Lu W, Huang Q, Huang M, Li C, Chen W. Copper sulfide nanoparticles for photothermal ablation of tumor cells. *Nanomedicine*. 2010; 5:1161–1171. [PubMed: 21039194]
14. Zhou M, Zhang R, Huang M, Lu W, Song S, Melancon MP, Tian M, Liang D, Li C. A chelator-free multifunctional [64Cu]CuS nanoparticle platform for simultaneous micro-PET/CT imaging and photothermal ablation therapy. *J Am Chem Soc*. 2010; 132:15351–15358. [PubMed: 20942456]
15. Ji XJ, Shao RP, Elliott AM, Stafford RJ, Esparza-Coss E, Bankson JA, Liang G, Luo ZP, Park K, Markert JT, Li C. Bifunctional gold nanoshells with a superparamagnetic iron oxide-silica core suitable for both MR imaging and photothermal therapy. *J Phys Chem C*. 2007; 111:6245–6251.
16. Yung JP, Shetty A, Elliott A, Weinberg JS, McNichols RJ, Gowda A, Hazle JD, Stafford RJ. Quantitative comparison of thermal dose models in normal canine brain. *Med Phys*. 2010; 37:5313–5321. [PubMed: 21089766]
17. Stafford RJ, Fuentes D, Elliott AA, Weinberg JS, Ahrar K. Laser-induced thermal therapy for tumor ablation. *Crit Rev Biomed Eng*. 2010; 38:79–100. [PubMed: 21175405]
18. Lal S, Clare SE, Halas NJ. Nanoshell-enabled photothermal cancer therapy: impending clinical impact. *Acc Chem Res*. 2008; 41:1842–1851. [PubMed: 19053240]
19. Huang X, El-Sayed IH, El-Sayed MA. Applications of gold nanorods for cancer imaging and photothermal therapy. *Methods Mol Biol*. 2010; 624:343–357. [PubMed: 20217607]
20. Hu M, Chen J, Li ZY, Au L, Hartland GV, Li X, Marquez M, Xia Y. Gold nanostructures: engineering their plasmonic properties for biomedical applications. *Chem Soc Rev*. 2006; 35:1084–1094. [PubMed: 17057837]
21. Liang HP, Wan LJ, Bai CL, Jiang L. Gold hollow nanospheres: Tunable surface plasmon resonance controlled by interior-cavity sizes. *J Phys Chem B*. 2005; 109:7795–7800. [PubMed: 16851906]
22. Prevo BG, Esakoff SA, Mikhailovsky A, Zasadzinski JA. Scalable routes to gold nanoshells with tunable sizes and response to near-infrared pulsed-laser irradiation. *Small*. 2008; 4:1183–1195. [PubMed: 18623295]
23. Lu W, Zhang G, Zhang R, Flores LG 2nd, Huang Q, Gelovani JG, Li C. Tumor site-specific silencing of NF-kappaB p65 by targeted hollow gold nanosphere-mediated photothermal transfection. *Cancer Res*. 2010; 70:3177–3188. [PubMed: 20388791]
24. Zhang HF, Maslov K, Stoica G, Wang LHV. Functional photoacoustic microscopy for high-resolution and noninvasive in vivo imaging. *Nat Biotechnol*. 2006; 24:848–851. [PubMed: 16823374]
25. Lu W, Huang Q, Ku G, Wen X, Zhou M, Guzatov D, Brecht P, Su R, Oraevsky A, Wang LV, Li C. Photoacoustic imaging of living mouse brain vasculature using hollow gold nanospheres. *Biomaterials*. 2010; 31:2617–2626. [PubMed: 20036000]
26. Lu, W.; Melancon, M.; Xiong, C-Y.; Huang, Q.; Elliott, A.; Stafford, J.; Ku, G.; Gelovani, JG.; Li, C. World Molecular Imaging Congress; Kyoto, Japan. 2010.
27. Siegrist W, Solca F, Stutz S, Giuffre L, Carrel S, Girard J, Eberle AN. Characterization of receptors for alpha-melanocyte-stimulating hormone on human melanoma cells. *Cancer Res*. 1989; 49:6352–6358. [PubMed: 2804981]
28. Harisinghani MG, Barentsz J, Hahn PF, Deserno WM, Tabatabaei S, van de Kaa CH, de la Rosette J, Weissleder R. Noninvasive detection of clinically occult lymph-node metastases in prostate cancer. *N Eng J Med*. 2003; 348:2491–U5.
29. Melancon M, Lu W, Li C. Gold-based magneto/optical nanostructures: Challenges for in vivo applications in cancer diagnostics and therapy. *Mater Res Bull*. 2009; 34:415–421. [PubMed: 20582234]
30. Kim J, Park S, Ji EL, Jin SM, Lee JH, Lee IS, Yang I, Kim JS, Kim SK, Cho MH, Hyeon T. Designed fabrication of multifunctional magnetic gold nanoshells and their application to magnetic resonance imaging and photothermal therapy. *Angew Chem Int Ed*. 2006; 45:7754–7758.
31. Wang LY, Bai JW, Li YJ, Huang Y. Multifunctional nanoparticles displaying magnetization and near-IR absorption. *Angew Chem Int Ed*. 2008; 47:2439–2442.

32. Wang H, Brandl DW, Le F, Nordlander P, Halas NJ. Nanorice: a hybrid plasmonic nanostructure. *Nano Lett.* 2006; 6:827–832. [PubMed: 16608292]
33. Stöber W, Fink A, Bohn E. Controlled growth of monodisperse silica spheres in the micron size range. *J Colloid Interface Sci.* 1968; 26:62–69.
34. Park K, Liang G, Ji X, Luo ZP, Li C, Croft MC, Markert JT. Structural and magnetic properties of gold and silica doubly coated Fe<sub>2</sub>O<sub>3</sub> Nanoparticles. *J Phys Chem C.* 2007; 111:18512–18519.
35. Melancon MP, Lu W, Meng Z, Zhou M, Liang G, Elliott AM, Hazle JD, Myers JN, Li C, Stafford RJ. Targeted multi-functional gold-based nanoshells for MR-guided laser ablation of head and neck cancer. *Biomaterials.* 2011 in press.
36. Melancon MP, Elliott A, Ji X, Shetty A, Yang Z, Tian M, Taylor B, Stafford RJ, Li C. Theranostics with multifunctional magnetic gold nanoshells: photothermal therapy and t<sub>2</sub>\* magnetic resonance imaging. *Invest Radiol.* 2011; 46:132–140. [PubMed: 21150791]
37. Li YB, Lu W, Huang Q, Huang M, Chen W, Li C. CuS nanoparticles for photothermal ablation of tumor cells. *Nanomed.* 2010; 5:1161–1171.
38. Choi HS, Liu W, Misra P, Tanaka E, Zimmer JP, Ity Ipe B, Bawendi MG, Frangioni JV. Renal clearance of quantum dots. *Nat Biotechnol.* 2007; 25:1165–70. [PubMed: 17891134]
39. Ku, G.; Zhou, M.; Zhong, M.; Hazle, J.; Gelovani, J.; Li, C. World Molecular Imaging Congress; Kyoto, Japan. 2010.
40. Obata A, Kasamatsu S, Lewis JS, Furukawa T, Takamatsu S, Toyohara J, Asai T, Welch MJ, Adams SG, Saji H, Yonekura Y, Fujibayashi Y. Basic characterization of <sup>64</sup>Cu-ATSM as a radiotherapy agent. *Nucl Med Biol.* 2005; 32:21–28. [PubMed: 15691658]
41. You J, Zhang G, Li C. Exceptionally high payload of doxorubicin in hollow gold nanospheres for near-infrared light-triggered drug release. *ACS Nano.* 2010; 4:1033–41. [PubMed: 20121065]
42. You J, Shao R, Wei X, Gupta S, Li C. Near-infrared light triggers release of paclitaxel from biodegradable microspheres: photothermal effect and enhanced antitumor activity. *Small.* 2010; 6:1022–1031. [PubMed: 20394071]
43. Wu G, Mikhailovsky A, Khant HA, Fu C, Chiu W, Zasadzinski JA. Remotely triggered liposome release by near-infrared light absorption via hollow gold nanoshells. *J Am Chem Soc.* 2008; 130:8175–8177. [PubMed: 18543914]
44. Elbashir SM, Harborth J, Lendeckel W, Yalcin A, Weber K, Tuschl T. Duplexes of 21-nucleotide RNAs mediate RNA interference in cultured mammalian cells. *Nature.* 2001; 411:494–498. [PubMed: 11373684]

## Biographies

**Marites Melancon** is an Instructor in the Department of Imaging Physics at The University of Texas MD Anderson Cancer Center, working on the synthesis and characterization of novel multifunctional contrast and therapeutic agents for cancer. She earned her B.S. in chemistry from the University of San Carlos (Philippines) and her M.S. in chemistry from Ateneo de Manila University (Philippines). She received her Ph.D. in biomedical science, majoring in biochemistry and cancer biology, in 2007 from The University of Texas Health Science Center at Houston.

**Min Zhou** received his B.S. and Ph.D. in chemistry from Shandong University (China) in 1999 and 2006, respectively. He is currently a postdoctoral fellow in the Department of Experimental Diagnostic Imaging at The University of Texas MD Anderson Cancer Center. His research is focused on cancer diagnosis, targeting, and therapy using CuS nanoparticles.

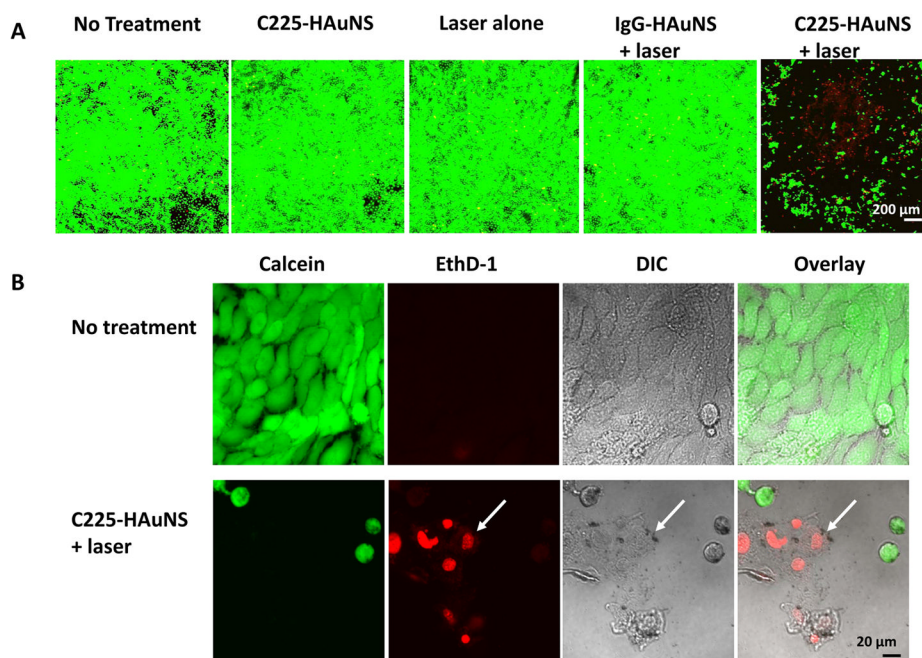
**Chun Li** is a Professor in the Department of Experimental Diagnostic Imaging at The University of Texas MD Anderson Cancer Center. Research in Dr. Li's laboratory is primarily focused on two areas: (i) developing targeted imaging probes for noninvasive characterization of molecular events associated with tumor progression and regression, and (ii) developing novel drug delivery systems for selective delivery of diagnostic and

therapeutic agents. He earned his Ph.D. in chemistry at Rutgers, The State University of New Jersey and his undergraduate degree from Peking University (China).

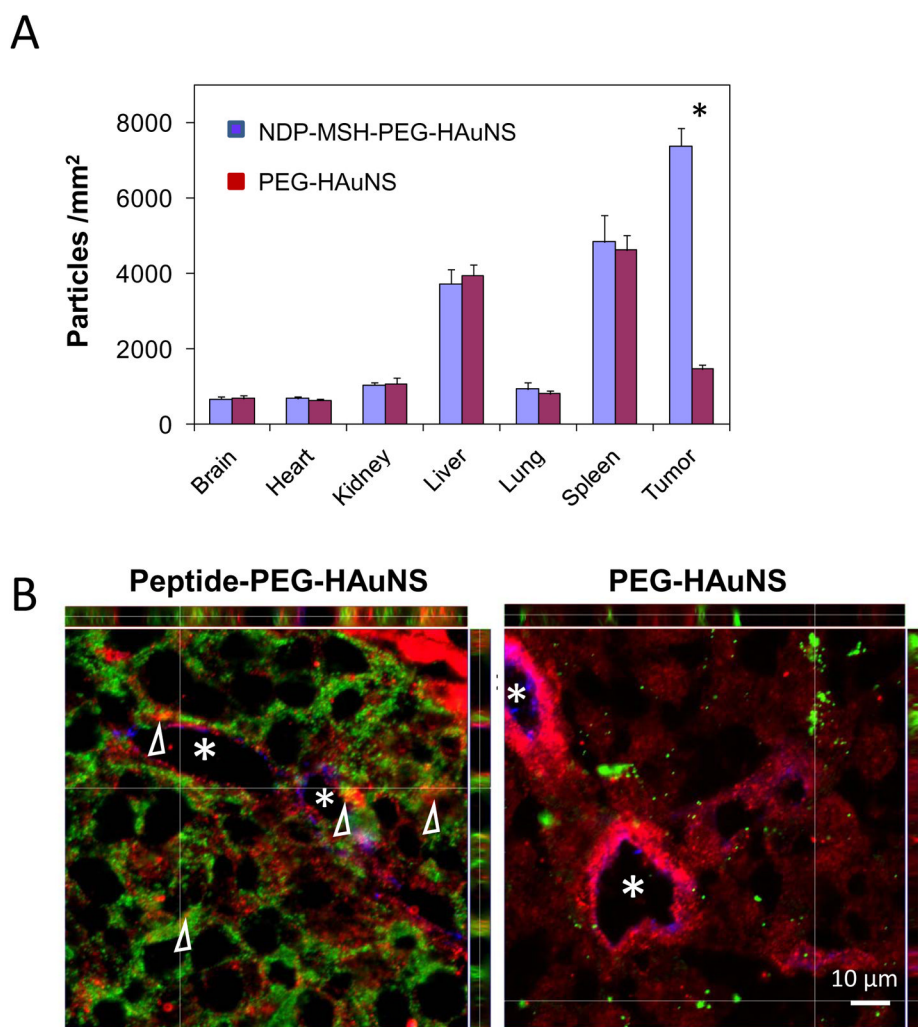
Nanoparticles	Structure	Imaging	Therapy	References
HAuNS		PET, PAT	PTA	11, 12, 23, 25
SPIO@Au NP		MRI	Thermal ablation	15, 35, 36
CuS NP		PET, PAT	Thermal ablation, radiotherapy	13, 14
Dox@PEG-HAuNS		PET, Optical	Thermal ablation, drug release	41
siRNA-HAuNS		PET, PAT	Thermal ablation, radiotherapy	23

**FIGURE 1.**

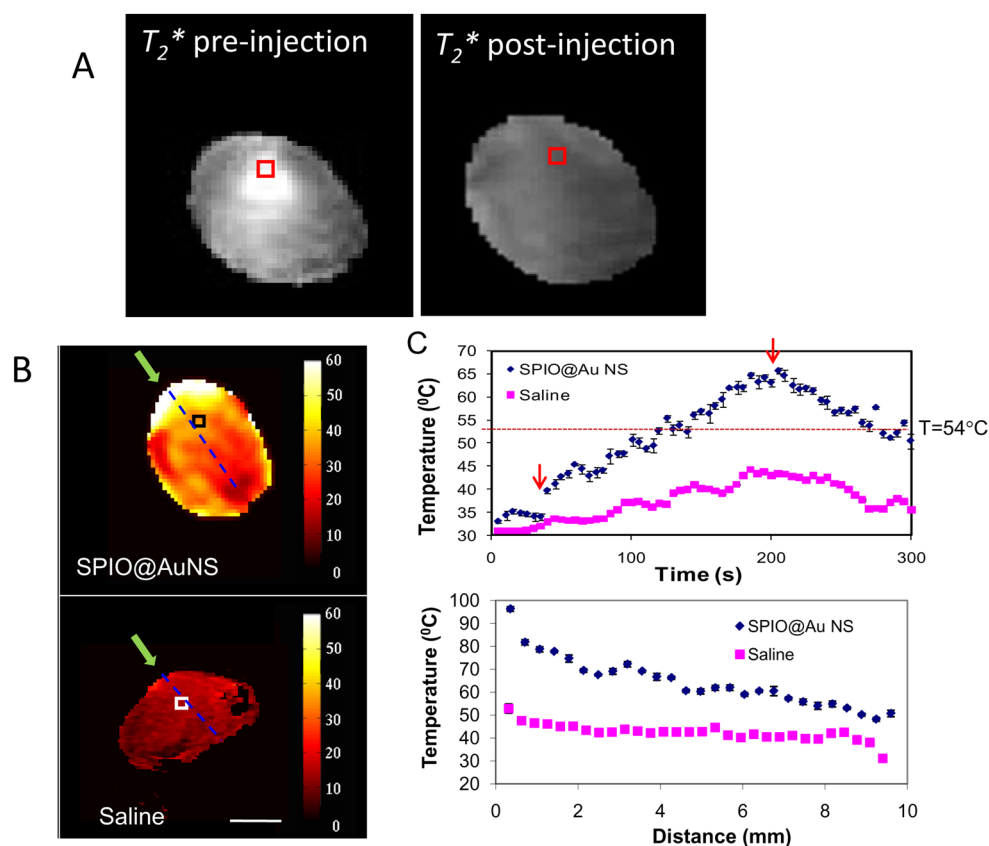
Structures and functions of near-infrared light-activatable theranostic nanoparticles. HAuNSs, hollow gold nanospheres; SPIO, superparamagnetic iron oxide; DOX, doxorubicin; CuS, copper sulfide; NP, nanoparticle; PTA, photothermal ablation; RNAi, RNA interference; siRNA, small interfering RNA; PET, positron emission tomography; PAT, photoacoustic tomography; MRI, magnetic resonance imaging.



**FIGURE 2.** Selective PTA of A431 cells by C225-HAuNSs. (A) Cell viability after various treatments. Viable cells were stained green with calcein AM and dead cells were labeled red with EthD-1. Magnification,  $\times 40$ . (B) Images of untreated viable cells and dead cells treated with C225-HAuNS and NIR laser at higher magnification ( $\times 400$ ). The dead cells are shown by positive staining with EthD-1 (arrow, red). DIC, differential interference contrast. (Reproduced with permission from Ref. 12)



**FIGURE 3.** Biodistribution and intratumoral distribution of FITC-tagged HAuNSs. Tissue and tumors were removed 24 h after intravenous injection of HAuNSs. (A) Biodistribution data calculated as the number of particle aggregates per square millimeter of visual area at magnification  $\times 200$ . Values are presented as mean  $\pm$  SD ( $n = 5$ ). \*,  $P < 0.01$ . (B) Representative fluorescence micrographs of cryosectioned B16/F10 melanoma. Melanocortin type-1 receptor was stained with rabbit anti-mouse melanocortin type-1 receptor polyclonal antibody (pseudocolored red). Blood vessels were stained with rat anti-mouse CD31 monoclonal antibody (pseudocolored blue). NDP-MSH-PEG-HAuNSs are pseudocolored green. White arrowheads, melanocortin type-1 receptor. Asterisks, the lumens of tumor vasculature. (Reproduced with permission from Ref. 11)

**FIGURE 4.**

(A) Representative  $T_2^*$ -weighted MRI scans of mice bearing A431 tumors before and after injection of SPIO@silica-Au NPs. (B) In vivo MRTI of a tumor injected intratumorally with SPIO@silica-Au NPs (top) and saline (bottom). At 24 h after injection of the agents, A431 tumors were irradiated with an 808-nm laser. Green arrows indicate the light path. Bar, 5 mm. (C) Temperature versus time for treatment volumes indicated by squares in (A), from 30 s before laser treatment (180 s, 4 W/cm<sup>2</sup>) until 90 s after laser treatment. Only in tumors injected with SPIO@silica-Au NPs was the temperature elevated above the 54°C threshold (dotted line) to ensure irreversible PTA of tumor cells. Arrows indicate when the laser was switched on and off. Values are presented as mean  $\pm$  SD. (D) Representative plot of temperature versus depth below tumor surface. (Reproduced with permission from Ref. 36)

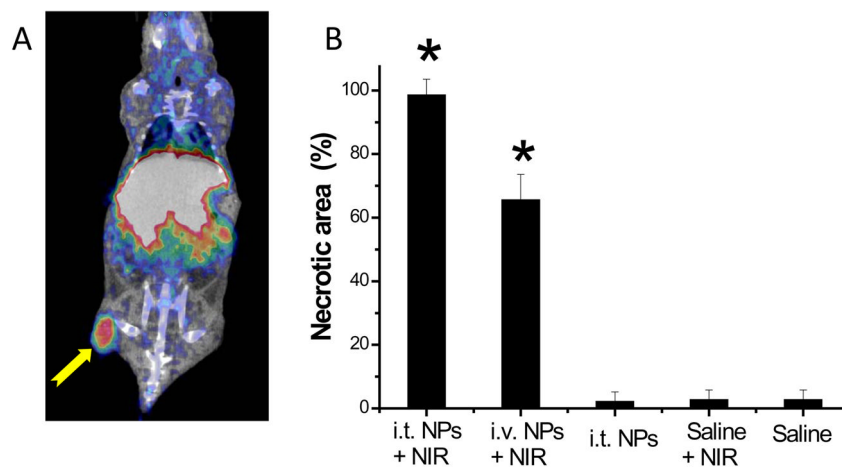


**FIGURE 5.**

(A) MicroPET/CT image of nude mouse bearing subcutaneous U87 glioma xenograft, acquired at 24 h after intravenous injection of PEG- $^{64}\text{Cu}$ CuS NPs. Arrow: tumor. (B) CuS NPs induced PTA destruction of tumors in vivo at 24 h after NIR laser irradiation (12 W/cm<sup>2</sup> at 808 nm for 5 min). i.v., intravenous; i.t., intratumoral. Values are presented as mean  $\pm$  SD. Asterisks,  $p < 0.001$  compared to saline only control. (Figure reproduced with permission from Ref. 14)

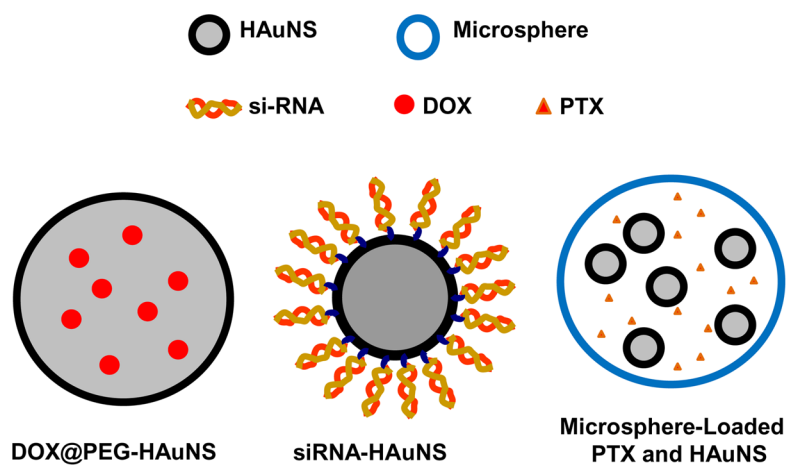


**FIGURE 6.** Schematic representation of the different NIR-activatable drug delivery systems.

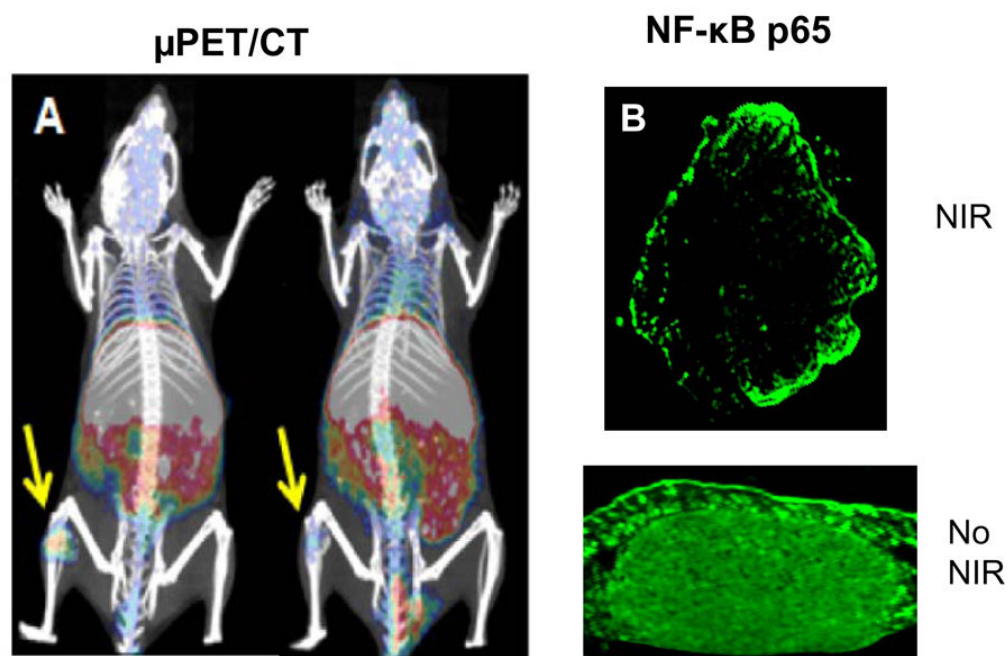


**FIGURE 7.** (A) MicroPET/CT images of mice bearing subcutaneous HeLa cells after intravenous injection of  $^{64}\text{Cu}$ -FA-HAuNS-siRNA<sub>NF- $\kappa$ B</sub> (left) and HAuNS-siRNA<sub>NF- $\kappa$ B</sub> (control, right). Arrows: tumors. (B) NF- $\kappa$ B p65 expression in tumors exposed (top) and not exposed (bottom) to NIR laser. (Reproduced with permission from Ref. 23)